Int. J. Non-Linear Mechanics, Vol. 25, No. 4, pp. 417–432, 1990
Printed in Great Britain.

0020–7462/90 $3.00 + .00
Pergamon Press plc

BIFURCATIONS AND CHAOS IN A FORCED ZERO-STIFFNESS IMPACT OSCILLATOR

G. X. LI,† R. H. RAND* and F. C. MOON†

*Department of Theoretical and Applied Mechanics, †Sibley School of Mechanical and Aerospace Engineering, Cornell University, Ithaca, NY 14853, U.S.A.

(*Received* 13 *January* 1989)

Abstract—We study a simple model of a structure having a pin joint with "play". The model consists of a zero-stiffness impact oscillator. For small forcing we analyse two types of simple periodic solutions: symmetric and asymmetric. Saddle-node and pitchfork bifurcations are found for both types of solutions, while period-doubling bifurcations are found for the asymmetric periodic solutions. For large forcing it is numerically shown that the system exhibits chaos.

1. INTRODUCTION

In this paper we discuss the bifurcation analysis and chaotic behavior of a simple mechanical oscillator, the study of which is motivated by an earlier study of space truss structures with smooth pin joints [1].

In contrast to welded joints which make a structure relatively rigid, pin joints permit a structure to have a certain degree of "play". In [1] it was found that forced oscillation of a pinned truss structure consisting of 147 aluminum bar members led to a chaotic response. The present work was motivated by the question of whether the source of the chaos was the large number of elements in the experimental truss, or whether chaos would result from forcing a small structure which was held together by pin joints. In order to separate the question of the complexity of the structure from the question of its having pin joints, we propose the following model of a single pin joint.

We imagine two truss members to be joined by a smooth pin with play (as in Fig. 1). For simplicity, and in order to define the problem clearly, we assume that one of the members is fixed in a Newtonian frame, and the other member is constrained to translate along a straight line. We assume that the pin is attached to the movable member, and that the play comes from the size of the slot in the fixed member being larger than the size of the pin which fits into it.

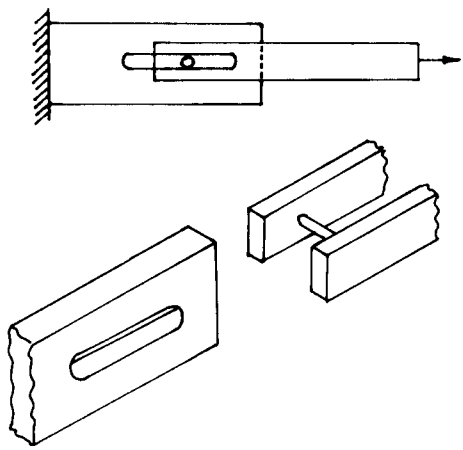

Fig. 1. Two truss members joined by a smooth pin with play.

In response to a force F as in Fig. 1, the movable member will encounter no resistance except inertia until the pin reaches the end of the slot. We model the impact of the pin on the fixed member as an *inelastic* collision, so that if the velocity of the moveable member was v before the collision, it will be $-rv$ after the collision, where $r < 1$ is a coefficient of restitution.

If we take the force F to be sinusoidal and let x measure the position of the pin, the system is governed by the following nondimensional differential equation and boundary conditions:

$$x'' = \gamma \sin t \quad \text{for } |x| < 1, \tag{1a}$$

$$x' \to -rx' \quad \text{for } |x| = 1, \tag{1b}$$

where γ is forcing amplitude. Unlike the usual linear oscillator, the system (1a) has no linear stiffness term. Although viscous damping has been omitted from equation (1a), the model exhibits energy loss due to the inelastic collision (1b). The system is invariant under the transformation

$$(x, x', t) \to (-x, -x', t + \pi).$$

Thus if $x = \varphi(t)$ is a solution, then $x = -\varphi(t + \pi)$ is also a solution. We call the system (1) a *zero-stiffness impact oscillator.*

In order to study the bifurcation of periodic solutions for this system, we first find the periodic solutions and then determine their stability. Rather than using the Floquet technique of computing characteristic multipliers for each periodic solution, we replace the flow (i.e. the solutions to the differential equation) by a discrete mapping called the Poincare map. In this way, a periodic solution in the original phase space becomes a fixed point in the Poincare map. The study of the stability of the periodic motion in the flow is equivalent to the study of the stability of the corresponding fixed point in the Poincare section, which is determined by the eigenvalues of the linearized Poincare map at the fixed point.

System (1) is equivalent to a free particle sliding in one dimension on a frictionless oscillating table and stopped by two walls fixed to the table (for an experimental model, see [7, p. 136]). If y represents the position of the particle relative to a fixed reference frame, then $y'' = 0$ and the walls are located at $y = \pm 1 + \gamma \sin t$. Choosing $x = y - \gamma \sin t$ to be the position of the particle relative to the table, we obtain the system (1). The present work is thus related to other recent studies of piecewise-liner impact oscillators [2–4]. Holmes [2] studied the dynamics of a bouncing ball repeatedly impacting with a sinusoidally vibrating table under the influence of gravity. The analysis in [2] was carried out directly on a discrete model (for more details, see [5]), rather than through differential equations and Poincare maps as in the present work. Another related study is the Fermi problem [6] which also involves a bouncing ball model treated by replacing the solution of the differential equations of motion by an approximate discrete model. Shaw and Holmes [3] and Shaw and Rand [4] have also worked on various models of impact oscillators. The approach used in the present work is similar to that used in [4] to study the dynamics of an inverted pendulum whose motion is limited by impacts with walls. The governing differential equation in [4] is, in contrast to equation (1a),

$$x'' - x = \gamma \sin t. \tag{2}$$

Thus the two systems are very different: the unperturbed ($\gamma = 0$) inverted pendulum has three equilibrium positions (an unstable one at the origin, and two stable ones at the resting points), while the unperturbed zero-stiffness oscillator has infinitely many equilibrium points.

In Section 2 we discuss the formulation of conditions for the existence of periodic solutions. In Section 3 we introduce the Poincare map for the system and then determine the eigenvalues of the map linearized about a periodic solution. By varying parameters, e.g. the driving amplitude, we can find the critical parameter values at which bifurcation occurs. In Section 4 the chaotic motion of the system due to large forcing is considered. Section 5 contains a summary of our results.

2. DETERMINATION OF PERIODIC SOLUTIONS

In order to present our results in the phase plane, we rewrite equation (1) as a set of first-order equations:

$$x' = y, \tag{3a}$$

$$y' = \gamma \sin t \quad \text{for } |x| < 1, \tag{3b}$$

$$y \to -ry \quad \text{for } |x| = 1, \tag{3c}$$

where x stands for displacement, and y for velocity of the oscillator. Note that the system (3) only contains two parameters: the driving amplitude γ and the restitution coefficient r. For a lightly damped system in which the energy loss is negligible during the impact, r is close to unity. For convenience in the following discussion, r will be fixed while γ is varied in order to investigate the dynamics of the system.

By a periodic solution of order n we shall mean a periodic solution which has a period n times the forcing period T (where n is an integer). There exist many different types of periodic solutions of order n. The simplest type is one in which impacts occur only once per cycle with each of the two boundaries, and which takes a time nT to complete a whole cycle ($T = 2\pi$ for our oscillator). Some periodic orbits may impact more than once with each boundary during a single cycle. Finding the general such solution is at best extremely difficult. In this paper we will consider only those periodic solutions which have a single impact with each of the boundaries during a single cycle, referred to as *simple periodic solutions*. Unlike the inverted pendulum oscillator [4], the type of periodic motion in which the oscillator impacts with only one of the two boundaries does not occur in our system.

To find a simple periodic solution, we assume that the oscillator starts at the boundary $x = +1$ with an initial velocity y_0 (as shown in Fig. 2). A complete cycle is as follows: The oscillator starts at $p_0 = (t_0, y_0)$ and immediately jumps to p_1 via the impact rule (1b). The subsequent motion is governed by the differential equation (1a), and the system moves to the left (since $y < 0$) until it reaches the boundary $x = -1$ at p_2, at which point it again jumps, this time to p_3. The oscillator continues its journey toward the right until it reaches the boundary $x = +1$ at p_4. If $p_4 = p_0$, then the orbit is a periodic one.

Within the simple periodic solutions, we have two different types of motions: *symmetric solutions* in which the oscillator spends an equal time between any two consecutive impacts, and *asymmetric solutions* in which the time spent going from p_1 to p_2 is unequal to the time spent going from p_3 to p_4. In the following, we shall consider these two kinds of simple periodic solutions separately.

2.1. *Symmetric solutions*

For the symmetric solutions of order n, we require the velocities at p_0 and p_2 to be equal in magnitude but opposite in sign: $y_2 = -y_0$. The subharmonic order n must be odd ($n = 1, 3, 5, \ldots$), which can be seen from the vector field $f = (y, \gamma \sin t)$. At p_0, $f_0 = (y_0, \gamma \sin t_0)$. When the system reaches p_2,

$$t = t_2 = t_0 + nT/2 = t_0 + n\pi,$$

$$\text{and} \quad f_2 = (y_2, \gamma \sin t_2) = (-y_0, \gamma \sin(n\pi + t_0)).$$

The symmetry condition on the velocities at p_0 and p_2 requires that $f_2 = -f_2$, or, $\sin(n\pi + t_0) = -\sin t_0$, which shows that n must be odd.

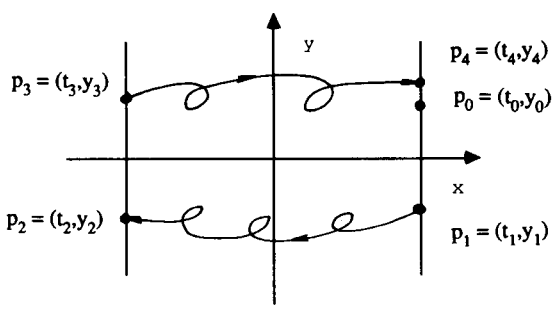

Fig. 2. A schematic diagram of the flow in the phase plane.

We ask for what values of γ can we find initial values t_0 and y_0 such that there exists a simple symmetric periodic solution. From p_0 to p_1, the oscillator undergoes an impact that reverses its direction: $y_1 = -ry_0, t_1 = t_0$. From p_1 to p_2, the solution to equations (3a) and (3b) is

$$x = c_1 + c_2(t - t_0) - \gamma \sin t, \tag{4a}$$

$$y = c_2 - \gamma \cos t, \tag{4b}$$

where c_1 and c_2 are two integration constants and are determined from the initial conditions at p_1:

$$c_1 = 1 + \gamma \sin t_1, \tag{5a}$$

$$c_2 = y_1 + \gamma \cos t_1. \tag{5b}$$

When $t = t_2 = t_0 + n\pi$ (n odd), the oscillator is required to reach the boundary $x = -1$, and we have

$$-1 = c_1 + c_2\Delta_{21} - \gamma \sin t_2 = c_1 + c_2\Delta_{21} + \gamma \sin t_0, \tag{6a}$$

$$-y_0 = c_2 - \gamma \cos t_2 = c_2 + \gamma \cos t_0, \tag{6b}$$

where $$\Delta_{21} = t_2 - t_1 = nT/2$$

is half the period of the response. Equations (5) and (6) involve $\sin t_0$, $\cos t_0$, and y_0, and can be solved to yield

$$4y_0^2(1 - r)^2 + [y_0(1 + r)\Delta_{21} - 4]^2 = 16\gamma^2, \tag{7a}$$

$$\sin t_0 = \frac{1}{4\gamma}[y_0(1 + r)\Delta_{21} - 4], \tag{7b}$$

$$\cos t_0 = -\frac{1}{2\gamma} y_0(1 - r),$$

from which t_0 and y_0 can be solved. Note that equation (7a) is a quadratic equation in y_0. Thus only for certain values of γ and r can y_0 have real solutions. This condition can be found by letting the discriminant of (7a) be zero:

$$\gamma \geq \gamma_c = \left[1 + \frac{\Delta_{21}(1 + r)^2}{4(1 - r)^2}\right]^{-1/2}. \tag{8}$$

Equation (8) represents a *saddle-node* bifurcation, as will be seen in the next section.

Figure 3 shows two typical periodic orbits for $n = 1$ and $n = 3$. When $n = 1$, $r = 0.5$, $\gamma = 0.20826$, solving (7) gives $t_0 = 3.27216$ and $y_0 = 0.82581$. When $n = 3$, $r = 0.5$, $\gamma = 0.08657$, (7) gives $t_0 = 2.5941$ and $y_0 = 0.29569$. Note that the average velocity of the motion for $n = 3$ in Fig. 3(b) is much smaller than that for $n = 1$ in Fig. 3(a). In fact, as seen from (7a), when $n \to \infty$ ($\Delta_{21} \to \infty$), for fixed γ, $y_0 \to 0$ so that the velocity of the motion becomes small for large n.

2.2. *Asymmetric solutions*

In the case of asymmetric simple periodic solutions, the oscillator spends an unequal length of time travelling to the right (in the upper half of the phase plane) vs travelling to the left (in the lower half of the phase plane). Here given γ, we want to find initial conditions corresponding to asymmetric simple periodic solutions of order n. The approach is similar to that of the symmetric case except that we have to consider a complete cycle from p_0 to p_1, p_2, p_3, and return to p_0.

From p_1 to p_2, the solution to equations (3a) and (3b) is again of the form (4) where (cf. (5, 6)):

$$-1 = c_1 + c_2\Delta_{21} - \gamma \sin t_2, \tag{10a}$$

$$y_2 = c_2 - \gamma \cos t_2, \tag{10b}$$

where c_1 and c_2 are given by (5). Similarly, from p_3 to p_4, we have

$$1 = c_3 + c_4\Delta_{43} - \gamma \sin t_4, \tag{11a}$$

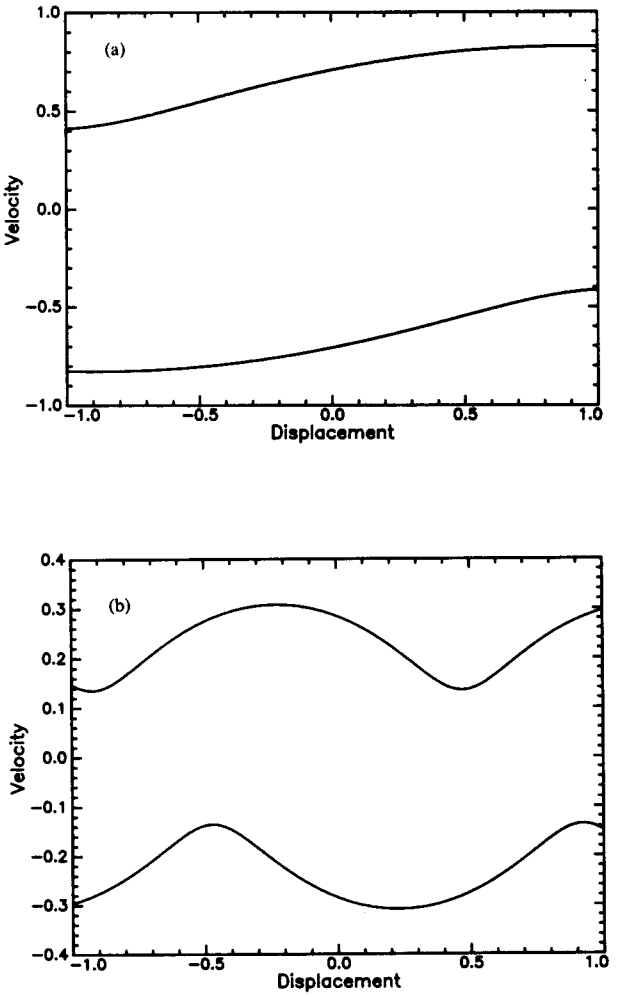

Fig. 3. Symmetric simple periodic motions in the x, y plane. (a) $n = 1$, $r = 0.5$, $\gamma = 0.20826$, $t_0 = 3.27216$, $y_0 = 0.82581$; and (b) $n = 3$, $r = 0.5$, $\gamma = 0.8657$, $t_0 = 2.5941$, $y_0 = 0.29569$.

$$y_4 = c_4 - \gamma \cos t_4 \tag{11b}$$

where

$$c_3 = -1 + \gamma \sin t_3$$

$$c_4 = y_3 + \gamma \cos t_3,$$

$$\Delta_{43} = t_4 - t_3.$$

For a periodic solution, $\sin t_4 = \sin t_0$, and $\cos t_4 = \cos t_0$. Using the impact rule (1b), $y_1 = -ry_0$, $y_3 = -ry_2$, and letting $y_4 = y_0$ in (11), we can solve for y_0 and y_2:

$$y_0 = -\gamma \cos t_0 - (a_2 - a_0 - 2)/\Delta_{43}, \tag{12a}$$

$$y_2 = [\gamma \cos t_2 + (a_2 - a_0 - 2)/\Delta_{43}]/r, \tag{12b}$$

where

$$a_i = \gamma \sin t_i \quad (i = 0, 2) \tag{13}$$

is the acceleration at time t_i. Substituting (12) into (10), and noting that $t_2 = t_0 + \Delta_{21}$, the quantities $\sin t_0$ and $\cos t_0$ can be solved for:

$$\sin t_0 = n_1/d, \tag{14a}$$

$$\cos t_0 = n_2/d, \tag{14b}$$

where

$$n_1 = 2[r\Delta_{43} - \Delta_{21} + (r\Delta_{21} - \Delta_{43})\cos\Delta_{21}],$$

$$n_2 = 2(r\Delta_{21} - \Delta_{43})\sin\Delta_{21},$$

$$d = \gamma(1 + r)[\Delta_{21}\Delta_{43}\sin\Delta_{21} + (\Delta_{21} - \Delta_{43})(1 - \cos\Delta_{21})].$$

Therefore, the condition for periodic solutions of order n can be written

$$n_1^2 + n_2^2 = d^2. \tag{15}$$

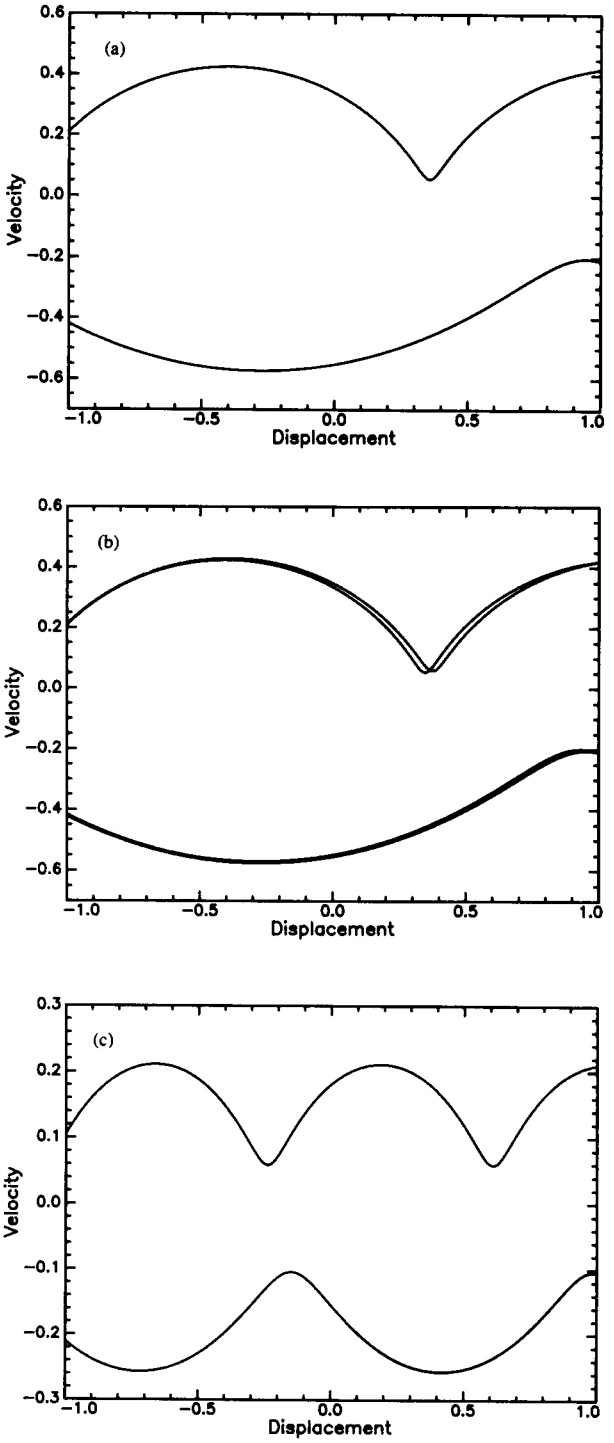

Fig. 4. (a–c).

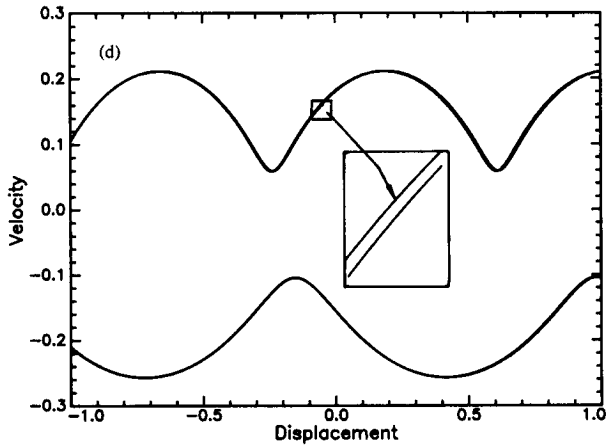

Fig. 4. Phase flows for the asymmetric motions demonstrating period-doubling phenomenon. Subharmonic order $n = 2$ for (a) and (b), and $n = 4$ for (c) and (d); $r = 0.5$.

When γ and r are given, (15) is a function of Δ_{21} and Δ_{43}. But $\Delta_{21} + \Delta_{43} = nT$ and thus for a given n, the values of Δ_{21} and Δ_{43} can be obtained numerically. Subsequently, t_0, y_0 and y_2 can be computed from (14) and (12). Two such periodic solutions for $n = 2$ and $n = 4$ are shown in Fig. 4(a) and (c).

3. STABILITY ANALYSIS AND BIFURCATIONS

A previous experimental study of a space truss structure with loose joints showed a chaotic response even when the truss was driven by sinusoidal forcing [1]. Where can chaos be hidden in a system as simple as (1), where, in principle, we know its solution for any given initial condition? In this section we want to answer this question by performing a stability and bifurcation analysis. We seek critical values of the forcing amplitude at which bifurcations (changes in the number or stability of the simple periodic motions) occur. The analysis consists of computing the Jacobian matrix of the Poincare map at the periodic orbits and finding the critical eigenvalues that have absolute value unity. Before we begin our analysis, we show a typical chaotic trajectory for (3) in Fig. 5, where no periodicity can be observed within a long time period.

3.1. *The Poincare map*

We rewrite equation (3) into an autonomous system by introducing a phase angle φ:

$$x' = y, \tag{16a}$$

$$y' = \gamma \sin \varphi \quad \text{for } |x| < 1, \tag{16b}$$

$$\varphi' = 1, \tag{16c}$$

$$y \to -ry \quad \text{for } |x| = 1, \tag{16d}$$

where $\varphi = t(\text{mod } 2\pi)$. After [4], we take the Poincare surface of section Σ to be

$$\Sigma = \{(x, y, \varphi) \in I \times R \times S | x = +1, y > 0\} = S \times R^+,$$

where $I = [-1, 1]$, and S is the circle of period 2π in our case. The Poincare map converts the original three-dimensional flow (two-dimensional phase plane plus one-dimensional time) into a two-dimesional discrete mapping. The Poincare section is coordinatized by the phase φ and velocity y:

$$P: \Sigma \to \Sigma, \text{ i.e. } (\varphi_0, y_0) \xrightarrow{P} (\varphi, y). \tag{17}$$

In words, P takes the point (φ_0, y_0) in Σ back to another point (φ, y) in Σ via the governing equation and the impact rule (1b). If the orbit is simple periodic, then $(\varphi, y) = (\varphi_0, y_0)$.

Suppose that a simple periodic orbit corresponds to a stable (attracting) fixed point Q in the Poincare map. Then as the parameters of the system (γ and r) are changed, there are

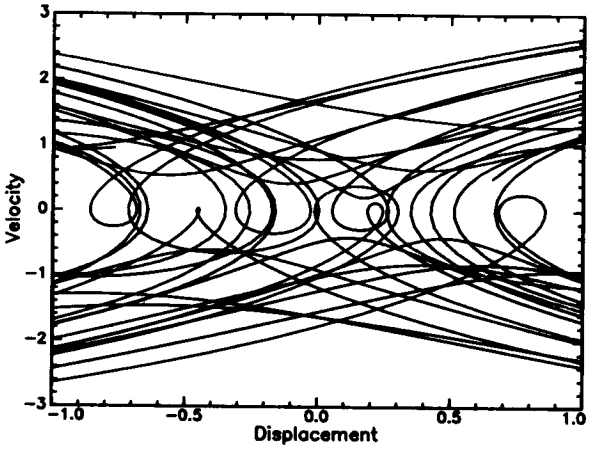

Fig. 5. An example of chaotic response in the x, y plane for $\gamma = 2.0$, $r = 0.9$, with initial condition $x_0 = y_0 = t_0 = 0$.

three elementary ways in which Q may become unstable: (a) one of the eigenvalues of the linearized Poincare map at the fixed point can become $+1$ (corresponding to a saddle-node or related bifurcation), (b) one of the eigenvalues can become -1 (corresponding to a flip or period-doubling bifurcation), or (c) a pair of complex eigenvalues can be have absolute value unity (corresponding to a Hopf bifurcation). As we will see, Hopf bifurcation is not possible in the present system. For a classification of bifurcations see Chapter 3 in [5].

As we will see later, an explicit form of Poincare map P cannot be obtained. However, our main objective in introducing P, the study of the stability of the simple periodic solutions, can be accomplished by using the implicit form of P.

To give the reader a qualitative feeling for the Poincare map for our system, we offer the results of numerical integration in Fig. 6 for $\gamma = 0.1$ and $r = 0.9$. The Poincare map was obtained by numerically solving equation (16) with initial conditions $x_0 = y_0 = t_0 = 0$, and recording the values of (t, y) whenever $x = +1$ and $y > 0$. Figure 6 was obtained by plotting $\varphi = t \pmod{2\pi}$ as abscissa and y as ordinate. Like other Poincare maps for chaotic motions, the first few points of this mapping looked quite random when observed on a computer screen, but eventually formed a highly ordered pattern (in contrast to true randomness). One should be aware that chaotic motions are often sensitive to their initial conditions. If the initial condition is changed, the motion may no longer be chaotic. We note that the Poincare map of Fig. 6 is similar to one experimentally obtained previously in a bouncing ball experiment (cf. [7, Figs 4–13, p. 137]).

3.2. *Saddle-node and pitchfork bifurcations for the symmetric solutions*

In order to determine the stability of a periodic solution emanating from (φ_0, y_0), we need to compute the Jacobian matrix of the Poincare map P at (φ_0, y_0):

$$DP(\varphi_0, y_0) = \frac{\partial(\varphi_4, y_4)}{\partial(\varphi_0, y_0)}. \tag{18}$$

To avoid confusion, we will still use t for φ in the following, keeping in mind that $\varphi = t \pmod{2\pi}$. Because of the discontinuity of the velocity y, the computation of the right hand side of (18) must be divided into four parts (see Fig. 2):

$$DP(t_0, y_0) = \frac{\partial(t_4, y_4)}{\partial(t_0, y_0)} = \frac{\partial(t_4, y_4)}{\partial(t_3, y_3)} \frac{\partial(t_3, y_3)}{\partial(t_2, y_2)} \frac{\partial(t_2, y_2)}{\partial(t_1, y_1)} \frac{\partial(t_1, y_1)}{\partial(t_0, y_0)}. \tag{19}$$

From the impact rule, we have

$$\frac{\partial(t_1, y_1)}{\partial(t_0, y_0)} = \frac{\partial(t_3, y_3)}{\partial(t_2, y_2)} = \begin{bmatrix} 1 & 0 \\ 0 & -r \end{bmatrix}. \tag{20}$$

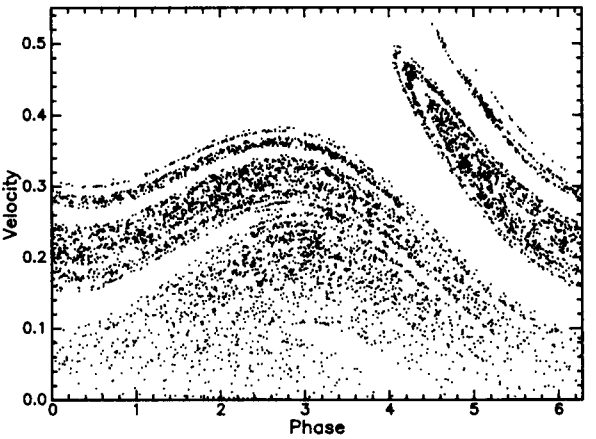

Fig. 6. A Poincare map in the section $\Sigma = \{(x, y, \varphi) | x = +1,\ y > 0, \text{ and } \varphi = t \pmod{2\pi}\}$ for $\gamma = 0.1$, $r = 0.9$, with initial condition $x_0 = y_0 = t_0 = 0$.

From p_1 to p_2, the flow is governed by differential equation, and t_2 and y_2 are related to t_1 and y_1 by

$$-1 = c_1 + c_2(t_2 - t_1) - \gamma \sin(t_2) \equiv f(y_1, t_1, t_2), \tag{21a}$$

$$y_2 = c_2 - \gamma \cos(t_2) \equiv g(y_1, t_1, t_2), \tag{21b}$$

where c_1 and c_2 are given by (5). A calculation of implicit derivatives for the functions f and g defined in (21) gives us

$$\frac{\partial(t_2, y_2)}{\partial(t_1, y_1)} = \begin{bmatrix} -\dfrac{\partial f}{\partial t_1} \div \dfrac{\partial f}{\partial t_2} & -\dfrac{\partial f}{\partial y_1} \div \dfrac{\partial f}{\partial t_2} \\ \dfrac{\partial g}{\partial t_2}\dfrac{\partial t_2}{\partial t_1} + \dfrac{\partial g}{\partial t_1} & \dfrac{\partial g}{\partial t_2}\dfrac{\partial t_2}{\partial y_1} + \dfrac{\partial g}{\partial y_1} \end{bmatrix} = \frac{1}{y_2}\begin{bmatrix} y_1 + a_1\Delta_{21} & -\Delta_{21} \\ a_1 a_2 \Delta_{21} + a_2 y_1 - a_1 y_2 & y_2 - a_2\Delta_{21} \end{bmatrix}. \tag{22}$$

The derivative $\partial(t_4, y_4)/\partial(t_3, y_3)$ from p_3 to p_4 can be obtained from the above matrix by replacing y_1 with y_3, y_2 with y_4, Δ_{21} with Δ_{43}, a_1 with a_3 and a_2 with a_4 (where $a_i = \gamma \sin t_i$, $i = 1, 2, 3, 4$). From the definition of the symmetric periodic motion and the impact rule we obtain the conditions

$$y_1 = -ry_0, y_2 = -y_0, y_3 = ry_0, y_4 = y_0,$$

$$a_1 = a_0, a_2 = -a_0, a_3 = -a_0, a_4 = a_0$$

and thus the Jacobian matrix of P at (t_0, y_0) has the form

$$DP = -\frac{1}{y_0^2}\begin{bmatrix} ry_0 - a_0\Delta_{21} & r\Delta_{21} \\ a_0 y_0(1 + r) - a_0^2\Delta_{21} & -r(y_0 - a_0\Delta_{21}) \end{bmatrix} \times \begin{bmatrix} -(ry_0 - a_0\Delta_{21}) & r\Delta_{21} \\ a_0 y_0(1 + r) - a_0^2\Delta_{21} & r(y_0 - a_0\Delta_{21}) \end{bmatrix}. \tag{23}$$

The eigenvalues of DP can be determined from

$$\lambda^2 - \operatorname{tr}\lambda + \det = 0, \tag{24}$$

where

$$\operatorname{tr} = -2r^2 + [2r - a_0\Delta_{21}(1 + r)/y_0]^2, \tag{25a}$$

$$\det = r^4 < 1. \tag{25b}$$

For λ complex, Hopf bifurcations require $|\lambda| = 1$ and hence cannot occur since det < 1. Saddle-node bifurcations occur for $\lambda = 1$, or

$$1 - \text{tr} + \det = 0. \tag{26}$$

Substituting the trace and determinant from (25) into (26) and using (7), we obtain the following two equilibria y_0:

$$y_{0_1} = \left[\frac{(1-r)^2}{\Delta_{21}(1+r)} + \frac{\Delta_{21}(1+r)}{4}\right]^{-1}, \tag{27a}$$

$$y_{0_2} = \frac{4\Delta_{21}}{(1+r)(\Delta_{21}^2 - 4)}, \tag{27b}$$

and from (7a), the corresponding critical values γ_c for the $\lambda = 1$ bifurcations are

$$\gamma_{c_1} = \left[1 + \frac{\Delta_{21}^2(1+r)^2}{4(1-r)^2}\right]^{-1/2}, \tag{28a}$$

$$\gamma_{c_2} = \frac{2[\Delta_{21}^2(1-r)^2 + 4(1+r)^2]^{1/2}}{(1+r)(\Delta_{21}^2 - 4)}. \tag{28b}$$

Note that γ_{c_1} is the same as (8), which corresponds to saddle-node bifurcations. When $\gamma < \gamma_{c_1}$, no equilibrium positions exist (equation (7a) has no real solutions), and when $\gamma > \gamma_{c_1}$, (7a) has two solutions. In the latter case, on one branch, both eigenvalues from (24) are positive and less than unity, implying stable equilibrium. On the other branch, one eigenvalue becomes larger than unity, implying that the equilibrium position is unstable. Figure 7(a) shows such a saddle-node bifurcation in the (γ, y) plane for $n = 1$. At the turning point, $(\gamma_{c_1}, y_{0_1}) = (0.20758, 0.8122)$, $\lambda = +1$. The curve was obtained by computing one solution of y_0 from (24) for $\lambda \in [0.85, 1.2]$, and then finding γ from (7a). It can also be obtained by solving for the two values of y_0 directly from (7a) for $\gamma \in [0.20758, 0.208]$. Similar saddle-node bifurcations also occur for large n (n odd).

The second critical value γ_{c_2} in equation (28b) corresponds to a pitchfork bifurcation. Unlike the saddle-node bifurcation, in this case the equilibrium exists for all γ in the neighborhood of γ_{c_2} (see Fig. 7(b) and (c) which applies to the case $n = 1$). The lower nearly-straight line in Fig. 7(b) is a solution for y_0 obtained from (24) for $\lambda \in [0.85, 1.2]$. At the bifurcation point, $(\gamma_{c_2}, y_{0_2}) = (0.7692, 1.4273)$, $\lambda = +1$. When $\gamma < \gamma_{c_2}$, both eigenvalues are positive and less than unity, resulting in a stable periodic orbit. When $\gamma > \gamma_{c_2}$, one of the eigenvalues becomes larger than unity and the orbit becomes unstable, denoted by a dashed line. In the latter case another stable orbit exists in the neighborhood of the unstable one. To find it, we can use the initial conditions (t_0, y_0) for the unstable orbits to simulate solutions from (3). The numerical solutions will slowly diverge from the unstable orbit represented by the dashed line, and will eventually converge to a stable orbit. The new numerically obtained stable orbit turns out to be a simple periodic orbit of the symmetric type for $n = 1$ and is obtainable analytically by the procedure described in Section 3.3. The values of y corresponding to points p_0 and p_2 (see Fig. 2) turn out to be equal, so that when displayed in Fig. 7(b), the new orbit appears as another solid line above the dashed line. In order to see the pitchfork bifurcation, we plot the travel times Δ_{21} and Δ_{43} as in Fig. 7(c). Similar pitchfork bifurcations also occur for large n (n odd).

Finally, the $\lambda = -1$ bifurcation turns out to be impossible in the present case because equation (24) has no real solutions for $\lambda = -1$.

3.3. *Saddle-node and period-doubling bifurcations for the asymmetric solutions*

In this section we compute the Jacobian matrix of the Poincare map associated with the asymmetric periodic solutions. This can be done in a similar fashion to the symmetric

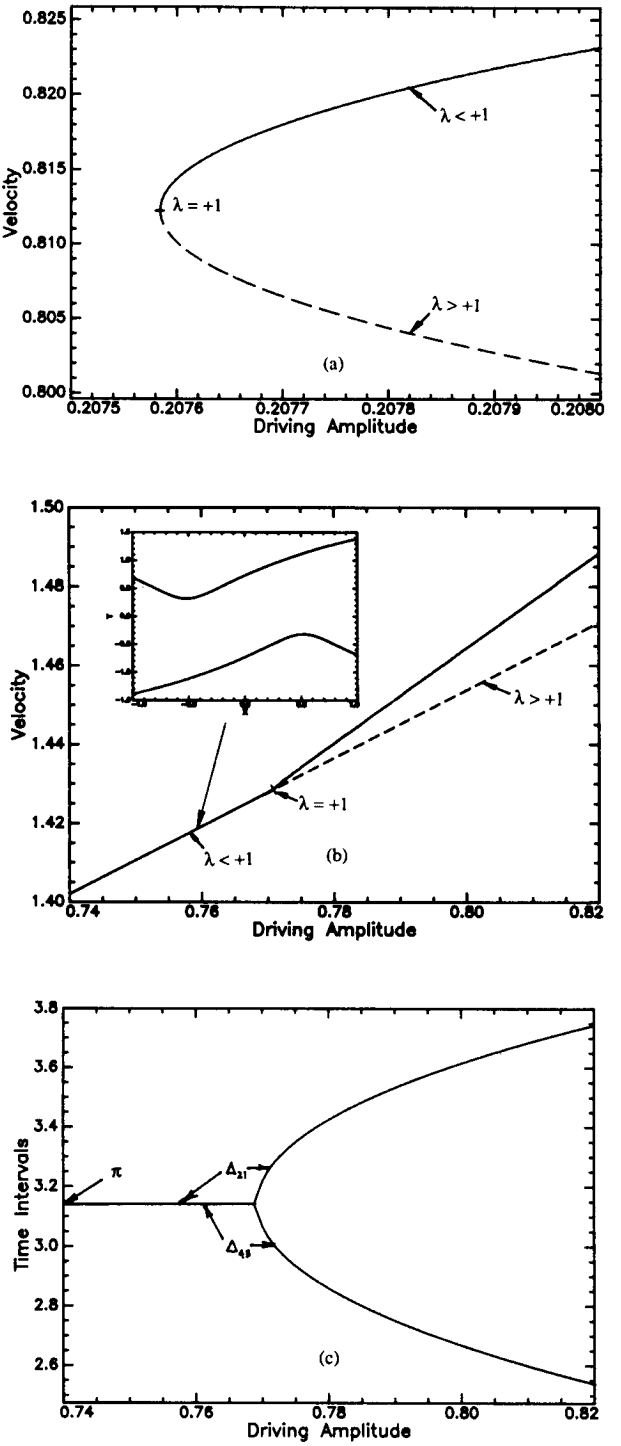

Fig. 7. $\lambda = +1$ bifurcations for the symmetric periodic motions at $x = +1$ for $r = 0.5$. (a) A saddle-node bifurcation, and (b), (c) a pitchfork bifurcation.

solutions. The result is

$$DP = \frac{1}{y_2 y_4}\begin{bmatrix} y_3 + a_3\Delta_{43} & r\Delta_{43} \\ a_3 a_4 \Delta_{43} + a_4 y_3 - a_3 y_4 & r a_4 \Delta_{43} - r y_4 \end{bmatrix} \times \begin{bmatrix} y_1 + a_1\Delta_{21} & r\Delta_{21} \\ a_1 a_2 \Delta_{21} + a_2 y_1 - a_1 y_2 & r a_2 \Delta_{21} - r y_2 \end{bmatrix}. \tag{29}$$

In this case, the velocities y_0 and y_2 are unrelated in general, and we have

$$y_1 = -ry_0, y_3 = -ry_2, y_4 = y_0,$$

$$a_1 = a_0, a_3 = a_2, a_4 = a_0.$$

Substituting the above quantities into (29), we obtain the trace and determinant

$$\text{tr} = 2r^2 - r(1+r)\Delta\left(\frac{a_0}{y_0} + \frac{a_2}{y_2}\right) + (1+r)^2\Delta_{21}\Delta_{43}\frac{a_0a_2}{y_0y_2}, \tag{30a}$$

$$\det = r^4 < 1, \tag{30b}$$

where $\Delta = \Delta_{21} + \Delta_{43} = nT$. Once again, $\det = r^4 < 1$, and no Hopf bifurcations can occur. The eigenvalues of (29) can be determined by substituting (30) into (24). At bifurcations, where $\lambda = +1$ or -1, no closed form expressions for the equilibria y_0 and y_2, and the critical values of γ, can be found (in contrast to equations (27) and (28) for the symmetric case). Nevertheless, these quantities, as well as the initial time t_0, can be solved for numerically. We outline the procedure here. Rewriting the condition (15) and the eigenvalue equation (24), we have

$$n_1^2 + n_2^2 - d^2 = 0, \tag{31a}$$

$$\lambda^2 - \text{tr}\,\lambda + \det = 0. \tag{31b}$$

Using the results in (12) and (14), and noting that $t_2 = t_0 + \Delta_{21}$ and $\Delta_{43} = 2nT - \Delta_{21}$, the above equations only involves two unknowns γ and Δ_{21} once the desired eigenvalue (i.e. $\lambda = +1$ or $\lambda = -1$) is given. The resulting equations can be easily solved numerically. The subsequent initial time t_0, and the equilibrium positions y_0 and y_2 can be computed from (14) and (12), respectively.

As in the symmetric case, $\lambda = +1$ again corresponds to a saddle-node bifurcation, with a bifurcation curve qualitatively the same as the one in Fig. 7(a). Our main interest for the asymmetric solutions is to investigate period-doubling bifurcations [8], which may be obtained by setting $\lambda = -1$ in (31b). As examples of such a bifurcation, Fig. 4 displays some phase flows for $n = 2$ and $n = 4$, when $r = 0.5$. When $n = 2$, we first set $\lambda = -0.75$ in (31b) and solve (31) yielding $\gamma = 0.18507$ and $\Delta_{21} = 0.7669$. From (12) and (14), $y_0 = -y_2 = 0.41915$, and $t_0 = 2.8705$. The trajectory in the (x, y) plane is shown in Fig. 4(a). We then set $\lambda = -1.25$ and repeat the calculation yeilding $\gamma = 0.18548$, $y_0 = -y_2 = 0.41944$, and $t_0 = 2.8474$. The trajectory corresponding to this set of values is unstable since $|\lambda| = 1.25$ which is larger than unity. Starting our numerical integration with these initial conditions, we see the system gradually diverge from the unstable asymmetric orbit and approach another stable periodic orbit (see Fig. 4(b)), which has period twice as long as the one in Fig. 4(a). A similar period-doubling sequence of periodic trajectories for $n = 4$ is shown in

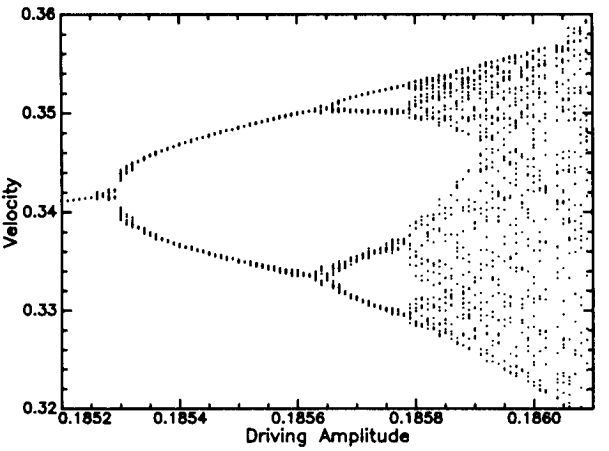

Fig. 8. Period-doubling bifurcation diagram for the asymmetric periodic motions in Fig. 4(a), (b) where $n = 2$. The ordinate represents steady state velocity y at $x = 0$.

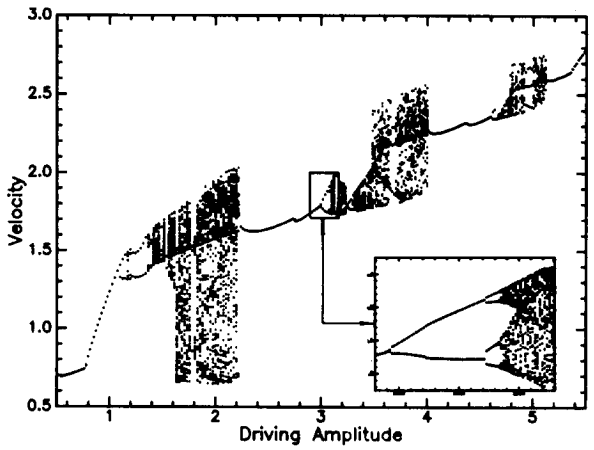

Fig. 9. Bifurcation diagram for large forcing amplitude; $r = 0.5$. Period-doubling, chaos, and sudden changes in velocities are observed. The ordinate represents steady state velocity y at $x = 0$.

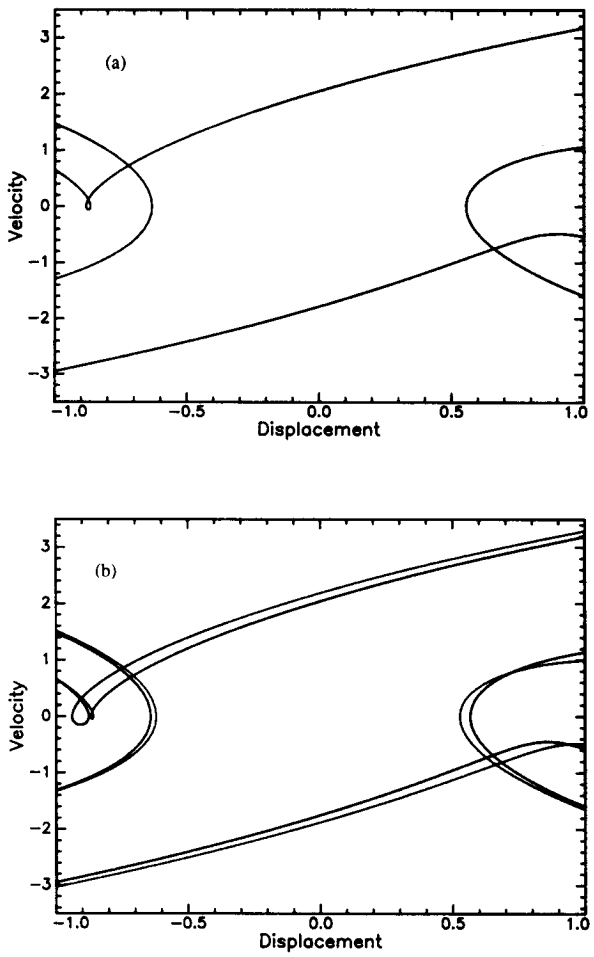

Fig. 10. Period-doubling in the phase plane for large forcing, $r = 0.5$. (a) $\gamma = 2.98$, (b) $\gamma = 3.05$.

Fig. 4(c) and (d). We note that in all these examples $y_0 = -y_2$ (although no such simple relationship exists between t_0 ad t_2).

Motivated by the period-doubling sequences in Fig. 4, we systematically simulated a period-doubling diagram for $n = 2$ and $r = 0.5$ (shown in Fig. 8). The period-doubling

cascade in the domain of $\gamma \in (0.1852, 0.1861)$ is recognizable, and the motion in the neighborhood of $\gamma = 0.1860$ is chaotic.

4. CHAOTIC MOTIONS DUE TO LARGE FORCING

In the previous section we found that the period-doubling cascade of asymmetric periodic solutions led to the onset of chaotic motions. The analysis was valid only for the simple

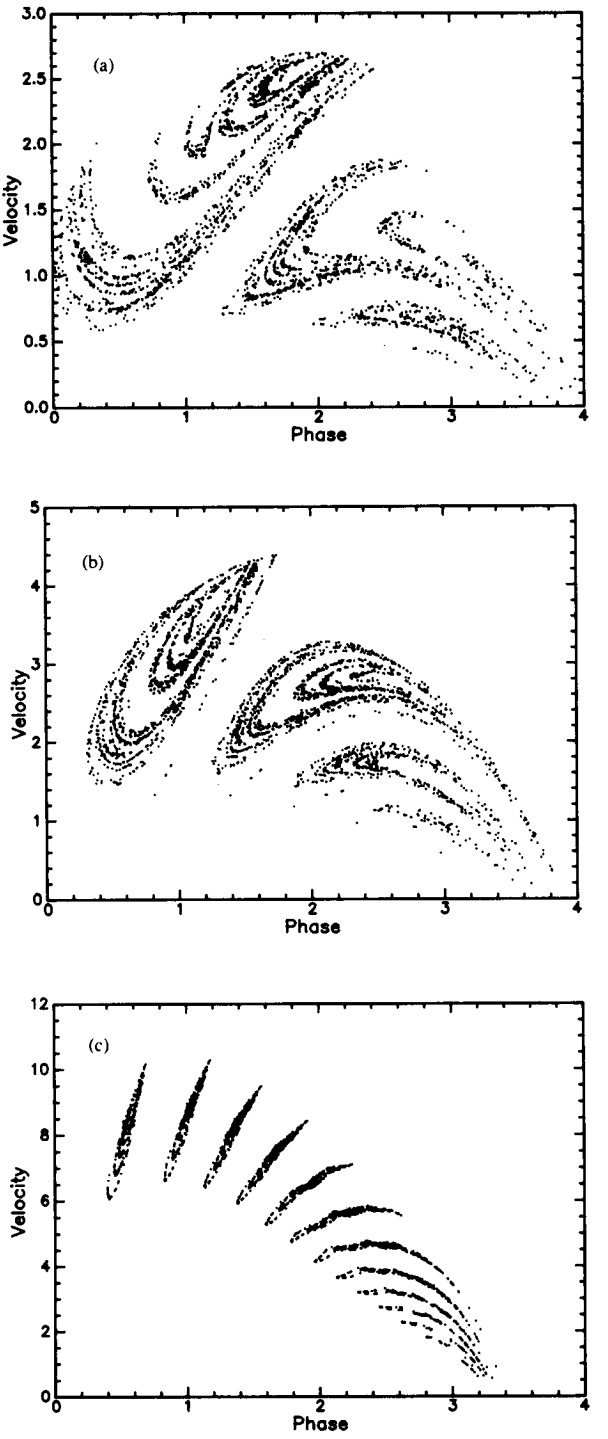

Fig. 11. Poincaré maps corresponding to large forcing for $r = 0.5$. (a) $\gamma = 2.0$, (b) $\gamma = 5.0$, and (c) $\gamma = 50.0$.

periodic motions, i.e. we assumed that the system strikes each of the two boundaries exactly once in a single cycle. The driving amplitude γ at which the bifurcation occurred was small ($\gamma < 0.5$). We have found that the higher the order n of the subharmonic, the smaller is the bifurcation value of γ. However, we have no knowledge about the nature of the motion under large forcing. The analysis in such a case involves determining periodic solutions with multiple impacts within a single cycle and the subsequent bifurcation analysis. Even with the use of computer algebra [9], which we employed to check the foregoing calculations, such an analysis is formidable. Here we only present some numerical results.

Figure 9 shows a bifurcation diagram for $\gamma \in [0.5, 5.5]$. The ordinate is the value of the velocity y at $x = 0$. There are three chaotic regions in this interval, and each of them is preceded by a period-doubling sequence and each ends suddenly with a crisis [7, 10]. To see this more clearly, we enlarged a small part of the diagram for $\gamma \in [2.98, 3.16]$, also shown in the same figure. This enlarged bifurcation diagram clearly demonstrates the period-doubling cascade, and is qualitatively the same as Fig. 8 (note that both have a larger spread at the lower branch). The stable equilibrium positions in the two intervals of $\gamma \in (2.2, 3.0)$ and $(4.0, 4.6)$ also have qualitatively the same shape: both have a kink in the middle. The bifurcation diagram in Fig. 9 was generated by dividing the interval $\gamma \in [0.5, 5.5]$ into 300 points $\{\gamma_i\}$, and numerically computing the steady state response of the system for each value of γ_i. For $\gamma_1 = 0.5$, an initial condition of $x_0 = 1.0$, $y_0 = 0.1$, and $t_0 = 0.0$ was used to simulate the solution. For all other amplitudes, $\gamma_i > 0.5$, the initial condition was taken to be the steady state values of (x, y, t) corresponding to the previous value of $\gamma = \gamma_{i-1}$.

Figures 10(a) and (b) shows two periodic orbits in phase space for $\gamma = 2.98$ and 3.05. In Fig. 10(a) the oscillator impacts twice with each of the boundaries during a single cycle. In Fig. 10(b), however, the period is doubled; the oscillator impacts four times with each of the boundaries during a single cycle.

Figure 11 shows three Poincare maps for $\gamma = 2$, 5 and 50 displayed on the Poincare section Σ discussed previously. As γ increases, the individual branches contract in size and additional branches emerge.

5. SUMMARY

This work was motivated by the use of pin joints in space truss structures and the appearance of chaos in the dynamics of such structures [1]. By investigating the dynamics of a system consisting of a single pin joint, we have been able to show that even systems with a small number of pin joints may be expected to be capable of complex dynamics.

In particular, we considered a special class of motions called simple periodic motions. By investigating the existence and stability of these motions we were able to predict the occurrence of a variety of bifurcations, including saddle-node, pitchfork and period-doubling. The latter led to a period-doubling cascade and chaos.

The simple periodic motions considered in this work represent but a small part of the total dynamics of the forced zero-stiffness impact oscillator. Numerical simulation has revealed that for large forcing amplitudes chaotic attractors are present in the system.

Acknowledgement—The authors would like to ackowledge helpful discussions with S. W. Shaw of Michigan State University.

REFERENCES

1. F. C. Moon and G. X. Li, Experimental study of chaotic vibrations in a pin-jointed space truss structure. To appear in *AIAA J.*
2. P. J. Holmes, The dynamics of repeated impacts with a sinusoidally vibrating table. *J. Sound Vib.* **84**, 173–189 (1982).
3. S. W. Shaw and P. J. Holmes, Periodically forced linear oscillator with impacts—chaos and long period motions. *Phys. Rev. Lett.* **51**, 623–626 (1983).
4. S. W. Shaw and R. H. Rand, The transition to chaos in a simple mechanical system. *Int. J. Non-linear Mech.* **24**, 41–56 (1989).
5. J. Guckenheimer and P. J. Holmes, *Nonlinear Oscillations, Dynamical Systems, and Bifurcations of Vector Fields.* Springer, New York (1983).

6. A. J. Lichtenberg and M. A. Lieberman, *Regular and Stochastic Motions*. Springer, New York (1983).
7. F. C. Moon, *Chaotic Vibrations*. Wiley, New York (1987).
8. M. Feigenbaum, Quantitative universality for a class of nonlinear transformations. *J. Stat. Phys.* **19**, 25–52 (1979).
9. R. H. Rand, Computer algebra in applied mathematics, in *Research Notes in Mathematics* **94**, Pitman, Boston (1984).
10. C. Grebogi, E. Ott and J. A. Yorke, Crises, sudden changes in chaotic attractors and transient chaos. *Physica* **7D**, 181–200 (1983).